Time-resolved Boson Emission in the Excitation Spectrum of $Bi_2Sr_2CaCu_2O_{8+\delta}$

J. D. Rameau,[1] S. Freutel,[2] M. A. Sentef,[3,4] A. F. Kemper,[5] J. K. Freericks,[6] I. Avigo,[2] M. Ligges,[2] L. Rettig,[2,†]
Y. Yoshida,[7] H. Eisaki,[7] J. Schneeloch,[1] R. D. Zhong,[1] Z. J. Xu,[1] G. D. Gu,[1] P. D. Johnson,[1] U. Bovensiepen[2]

[1]*Brookhaven National Laboratory, Upton, New York, 11973, USA**
[2]*Fakultät Für Physik und Zentrum für Nanointegration Duisburg-Essen, Universität Duisburg-Essen, Lotharstrasse 1, 47057 Duisburg, Germany*
[3]*HISKP, University of Bonn, 53115 Bonn, Germany*
[4]*Max Planck Institute for the Structure and Dynamics of Matter, Center for Free Electron Laser Science, 22761 Hamburg, Germany*
[5]*Lawrence Berkeley National Laboratory, 1 Cyclotron Road, Berkeley, CA 94720, USA*
[6]*Department of Physics, Georgetown University, Washington, DC 20057, USA*
[7]*National Institute of Advanced Industrial Science and Technology, Tsukuba, Ibaraki 305-8568, Japan and*
[†]*Current address: Swiss Light Source, Paul Scherrer Institute, 5232 Villigen PSI, Switzerland*

(Dated: May 27, 2015)

Using femtosecond time- and angle-resolved photoemission spectroscopy we analyze the complex unoccupied electronic structure of optimally doped $Bi_2Sr_2CaCu_2O_{8+\delta}$ after optical excitation. Electronic relaxation is characterized by a 250 fs relaxation time below and <20 fs above a single boson energy of ∼75 meV above the Fermi energy E_F which represents the unoccupied counterpart of the kink observed below E_F and T_c. With increasing optical excitation density this sharp energy-dependent step in the relaxation time is found to significantly weaken, in good agreement with self-energy and time-dependent Keldysh Green's function calculations, due to redistribution of electrons within the relaxation phase space. These findings have implications regarding the origin of the primary nodal kink in the electronic structure and for the mechanism behind high T_c superconductivity in the cuprates.

PACS numbers: 74.25.Jb 74.25.N- 74.72.Gh 78.47.J-

The origin and possible role in high T_c superconductivity of the nodal electronic mass renormalization, or dispersion "kink" in energy E and in-plane wavevector $k_\parallel$, first observed in optimally doped $Bi_2Sr_2CaCu_2O_{8+x}$ (Bi2212) using angle resolved photoelectron spectroscopy (ARPES), remains a central problem in the field of high T_c superconductivity in the cuprates [1]. Persistent interest in the nodal kink, located ~ 70 meV below the Fermi energy E_F, is due largely to the feature's universal prominence in the photoelectron spectrum of the cuprates[2] and the subtlety of its evolution across the phase diagram[3]. However, extensive study of the nodal kink's temperature, doping and momentum dependence [3, 4] with ever more refined analytical and experimental variations on the ARPES technique[5, 6] have not elucidated its origin or what role it might play in the wider high T_c problem. Observations of other dispersion kinks in the nodal [7, 8] and antinodal [9] regions of the Brillouin zone have only further confused these issues.

Leading candidates for the kink's origin are, respectively, an Eliashberg-type electron-boson interaction and a purely electronic energy scale originating in the strongly correlated nature of the cuprates. Discovering what mechanism produces the kink may, if it shares a related origin, resolve the fundamental question of high T_c superconductivity in the cuprates: whether Cooper pairing is induced by a bosonic "glue" or by purely electronic interactions descended from the cuprates' parent antiferromagnetic Mott insulating state[10]. The prime candidate bosons are in-plane Cu-O phonon modes [11] and spin excitations such as the (π, π) magnetic resonance first observed using neutron scattering [12]. Experimental evidence has also been put forth that the feature observed as a single nodal kink is in fact due to a confluence of several closely spaced phonon modes [13]. Strong correlation effects associated with the Marginal Fermi liquid phenomenology, charge and spin stripes or some more exotic mechanisms [14] have also been suggested as means to resolve various anomalies in the kink's relationship to the appearance of superconducting and pseudogap energy scales as temperature and doping are varied.

The addition of ultrafast laser excitation to photoemission allows such experiments to move from a static, passive mode to a time domain method in which electrons are rapidly kicked out of equilibrium and relaxation of their excited states is interrogated as a function of pump-probe delay time t. Recent trARPES studies of the nodal kink have revealed it to be profoundly weakened by ultrafast near-infrared laser excitation, though the optical pump fluence Φ required to effect such change is observed to be an order of magnitude larger above T_c than below [15, 16]. The time and fluence dependencies of this effect were subsequently explained as the result of a rearrangement of the population of filled and empty states within the "boson window" $-\hbar\Omega < E < +\hbar\Omega$ straddling E_F within which (at $T = 0$) no interactions with a single well-defined bosonic mode residing at $E = |\hbar\Omega|$ are allowed at equilibrium [17]. However, discrepancies between theoretical calculations for the weakening of the kink and the anomalous energy dependence of the changes in state momenta around E_F, intertwined with photodoping [15, 16] have left the boson description of the kink ambiguous.

While previous investigations revealed qualitatively new

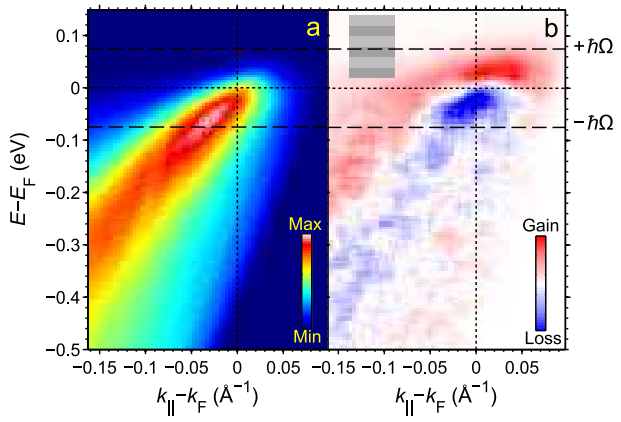

FIG. 1. (color online) a) Nodal $I(E, k_{||} - k_F, t_{(-)})$ at equilibrium, $t_{(-)}$ = -5 ps and equilibrium temperature T = 120 K. b) Difference spectrum $\Delta I = I(E, k_{\|} - k_F, t) - I(E, k_{\|} - k_F, t_{(-)})$ for $\Phi = 35\mu$J·cm^{-2}, t = 50 fs. Light and dark gray bars in panel b) depict energy bins ΔE centered at $E_{\rm bin}$ used to evaluate $I_{\rm norm}(E_{\rm bin}, t)$.

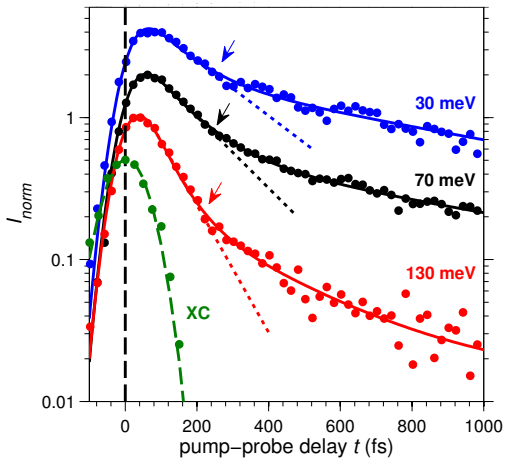

FIG. 2. (color online). $I_{\rm norm}(E_{\rm bin}, t)$ at $\Phi = 315\ \mu{\rm J}\cdot{\rm cm}^{-2}$ for $E_{\rm bin}$ = 30 meV (blue circles), 70 meV (black circles) and 130 meV (red circles), respectively, on a logarithmic intensity scale. Solid lines are fits to Eq. 1. Data for each $E_{\rm bin}$ are offset by a factor of two for clarity. Dotted lines are guides to the eye extending through $I_{\rm norm}(E_{\rm bin}, t)$ at times for which population decay is dominated by the scattering mechanism responsible for $\tau_{\rm short}$. Green points are from $I_{\rm norm}(E, t)$ integrated over all $k_{\|}$ and $1.45 < E < 1.5$ eV for $t < 200$ fs. The Gaussian fit to the green points (green dashed line) yields the XC width. Arrows denote time at which τ_{long} dominates $I_{\rm norm}(t)$.

phenomena in the cuprates, they haven't so far taken advantage of the technique's ability to populate and observe states above $E_{\rm F}$. In this Letter, we therefore turn to another, new and complementary, analysis of the trARPES spectrum of the normal state of optimally doped Bi2212. By energy-resolving relaxation times of electron populations photoexcited above $E_{\rm F}$ on time scales as fast as a few tens of femtoseconds, we demonstrate these carriers act as sensitive probes of the electron-boson interactions typically manifest as effective mass renormalizations in the occupied part of the spectrum. In particular, in Bi2212 *the photoexcited population displays the effects of scattering from a single sharp bosonic mode at an energy $+\hbar\Omega$ consistent with that of the main nodal kink observed below $E_{\rm F}$ at $-\hbar\Omega$.*

Our trAPRES experiment was performed on single crystals of optimally doped Bi2212 (T_c = 91 K) grown by the floating zone method. Samples were cleaved *in situ* at 100 K in a base vacuum of 5×10^{-11} Torr. Pump pulses of 800 nm wavelength and 40 fs duration, at 250 kHz repetition rate, were produced by a Coherent RegA 9040 regenerative amplifier. The 200 nm probe was produced as the fourth harmonic of part of the RegA's 800 nm fundamental [18]. The pump-probe cross-correlation (XC, Gaussian full width at half maximum) was 100 fs at the sample surface. Photoelectron spectra with an overall energy resolution of 55 meV, set by the bandwidth of the laser pulses, were recorded using both angle integrating time-of-flight (TOF) [18] and position sensitive TOF (pTOF) [19] electron spectrometers. The k resolution of the pTOF was 0.0025 Å^{-1} and the angular acceptance of the TOF was $\pm 3°$.

A typical equilibrium spectrum $I(E, k_{\|}, t_{(-)})$ of the nodal state recorded with the pTOF is shown in Fig. 1a. Here I is photoelectron intensity and $t_{(-)} = -5$ ps precedes the pump pulse. Though the dispersion kink is difficult to observe without spectral deconvolution at this resolution, the increase in coherence of the states between $-\hbar\Omega$ and $E_{\rm F}$ is still clear. Fig. 1b shows the difference spectrum $\Delta I(E, k_{\|}) = I(E, k_{\|}, t) - I(E, k_{\|}, t_{(-)})$ where $t = 50$ fs at $\Phi = 35\mu{\rm J}\cdot{\rm cm}^{-2}$. For this fluence, by $t = 50$ fs electrons excited above $+\hbar\Omega$ and holes injected below $-\hbar\Omega$ have largely relaxed while those within the boson window $-\hbar\Omega < E < +\hbar\Omega$ persist. Considering that the pump photon energy of 1.5 eV is well in excess of this $2\hbar\Omega$ range, our tracking of the excitations in the vicinity of $E_{\rm F}$ implies we're primarily observing scattered electrons and holes, and their relaxation towards $E_{\rm F}$, rather than the initial excitation. Fig. 1b shows the largest pump-induced intensity changes within the boson window. The existence of this pileup in excited carriers at finite t means relaxation times for carriers outside the boson window must be considerably shorter than inside since the former carriers have already relaxed by this time. Below, we show the difference in relaxation times in the unoccupied part of the spectrum above versus below $+\hbar\Omega$ results from the sudden change in phase space with increasing E for inelastic decay of excited carriers by emission of a single predominant bosonic mode. This conclusion is based upon quantitative agreement between our experiment and the theory of fluence-dependent relaxation times, revealing that dynamical repopulation of states modifies the phase space for relaxation of excited electrons by boson emission. Since this is process by which the previously observed melting of the kink below $E_{\rm F}$ was proposed to occur, we will argue that the present observations and modeling together imply the sharp kink at 70 meV must result from the coupling of electrons to a single well-defined bosonic mode below T_c.

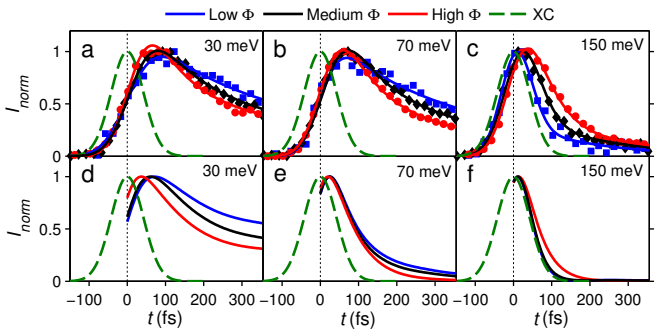

FIG. 3. (color online). a-c) $I_{\rm norm}$ for $E_{\rm bin} = 30$, 70 and 130 meV, respectively for $\Phi = 35$ (blue squares), 105 (black diamonds) and 315 (red circles) $\mu\mathrm{J}\cdot\mathrm{cm}^{-2}$. Solid lines in these panels are fits to Eq. 1. d-f) theoretical $I_{\rm norm}$ for the same $E_{\rm bin}$ as a-c for field strengths of 0.05 (blue), 0.15 (black) and 0.5 (red) in units of V/a where a is the Cu-Cu lattice constant[20]. a-f) Green dashed lines show the Gaussian XC.

To quantify these dynamical effects, we energy-resolve photoexcited intensity relaxation times τ above $E_{\rm F}$ in a manner that allows comparison to the equilibrium quasiparticle lifetime $\tau_{\rm QP}$ traditionally determined by ARPES. This is accomplished by dividing the trARPES spectrum into discrete energy bins of equal width $\Delta E = 20$ meV, Fig. 1b. Integrating the intensity within bins over $k_\parallel$ and ΔE results in time and energy dependent intensities $I_{\rm norm}(E_{\rm bin}, t)$, where $E_{\rm bin}$ is taken at the bin centers. Our analysis follows from observation of a pronounced biexponential decay of photoexcited carrier populations with respect to $E_{\rm bin}$ and Φ. Typical energy-resolved data for $\Phi = 315$ $\mu\mathrm{J}\cdot\mathrm{cm}^{-2}$ is shown in Fig. 2. On a log plot, normalized intensities $I_{\rm norm} = I(E_{\rm bin}, t)/\max[I(E_{\rm bin}, t)]$ are seen to decay with clearly separable short and long time components, the former lasting several hundred femtoseconds. Fits to $I_{\rm norm}(E_{\rm bin}, t)$ at fixed $E_{\rm bin}$ in Fig. 2, as well as all subsequent fits used to determine short and long exponential time constants $\tau_{\rm short}$ and $\tau_{\rm long}$, are performed using the model function

$$I_{\rm norm}(t) = \Theta(-t)(A_{\rm short}e^{-\frac{t}{\tau_{\rm short}}} + A_{\rm long}e^{-\frac{t}{\tau_{\rm long}}}) \otimes R_{\rm t} \quad (1)$$

where $\Theta(-t)$ is the Heaviside function, A's are intensities and $R_{\rm t}$ is a Gaussian of XC width. Though the form of the data requires two time constants, $\tau_{\rm short}$ and $\tau_{\rm long}$, detailed discussion of $\tau_{\rm long}$, whose origin is likely related to decay of carriers at all energies by emission of acoustic modes, was discussed previously [18]. ($\tau_{\rm long}(E_{\rm bin})$, and discussion of its effect upon fits to Eq. (1) is presented in the supplementary information.)

To facilitate examination of both energy and fluence dependencies of $\tau_{\rm short}$ we show representative $I_{\rm norm}(t)$ for several $E_{\rm bin}$ and Φ, and fits thereof, in Fig. 3a-c. The main trends in the data are the overall decrease in $\tau_{\rm short}$ with increasing $E_{\rm bin}$ for all fluences and the reversal in which fluence displays the fastest $\tau_{\rm short}$ as $E_{\rm bin}$ is increased past $+\hbar\Omega$. Indeed, plotting $\tau_{\rm short}(E_{\rm bin})$ for each fluence, Fig. 4a, shows a highly unusual relationship between the fluence dependence of $\tau_{\rm short}(E_{\rm bin})$ and whether $E_{\rm bin}$ is greater or less than $+\hbar\Omega$. At the lowest fluence $\tau_{\rm short}(E_{\rm bin})$ shows a pronounced step at $E_{\rm bin} \sim +\hbar\Omega$ with much shorter times above $+\hbar\Omega$ versus below. As pump fluence increases, relaxation times below $+\hbar\Omega$ decrease while those above $+\hbar\Omega$ increase. The step in $\tau_{\rm short}$ at $+\hbar\Omega$ for 35 $\mu\mathrm{J}\cdot\mathrm{cm}^{-2}$, which is reminiscent of the step in $\hbar/\tau_{QP}$ accompanying boson-induced mass renormalizations observed in ARPES [1, 21], has effectively the same origin. In ARPES, a single photohole injected above a bosonic mode energy has a shorter lifetime than one injected below because an additional interaction channel is open to the higher energy state, a phenomenon observed as a step in the imaginary part of the self energy. Likewise, electrons photoexcited above a bosonic mode's energy will decay faster than one excited to empty states below because the additional channel for energy loss due to boson emission is open to it. Indeed, this reciprocity in electron and hole lifetimes outside the boson window both above and below $E_{\rm F}$ is a textbook prediction of the theory of electron-boson coupling in solids, though this aspect of it hasn't to our knowledge been directly confirmed before [22].

While coincidence of the step in $\tau_{\rm short}$ at $+\hbar\Omega$ and the kink energy at $-\hbar\Omega$ is necessary to link these phenomena, it is the more complicated fluence dependencies of these phenomena that hold the key to resolving the nature of the nodal kink. As Φ is increased the dynamics of photoexcited carriers change from a regime reflecting essentially single-particle physics to one further characterized by the dynamics of populations of interacting, hot particles. The parallel evolution, with increasing fluence, of the broadening step in $\tau_{\rm short}$ on the one hand and the previously observed reduction in effective mass of the nodal kink below $E_{\rm F}$ on the other, therefore encourages a description of the former effects within the same theoretical framework as the latter [17]. To that end we have carried out model calculations of $I(E_{\rm bin}, t)$ for several pump field strengths with a theoretical machinery similar to that used previously to address the laser induced weakening of the kink [17, 23].

Energy relaxation of the excited carrier population is expected to occur on three distinct timescales [17]: (i) electron-electron (ee) thermalization on a femtosecond timescale; (ii) electron-boson thermalization on a tens to hundreds of femtoseconds timescale; and (iii) full system thermalization on picosecond or longer timescales. Here we focus on a phenomenological description of (ii), given experimentally by $\tau_{\rm short}$, which is described by a Holstein model coupling Bloch electrons to a single Einstein mode. Excited carriers relax via their coupling to this reservoir, which is assumed to have infinite heat capacity and thereby remains unchanged. Equilibrium $\tau_{\rm QP}(E)$ in Fig. 4b is generated by a single well-defined bosonic mode centered at $\hbar\Omega = 75$ meV. The dimensionless electron-boson coupling constant λ is chosen to be 0.2 to match relaxation times of order 20 fs at $E > \hbar\Omega$. We also note the same value for λ was found to bound the coupling of hot electrons to a particular subset of hot phonons in earlier trARPES experiments on Bi2212 [18]. The model also

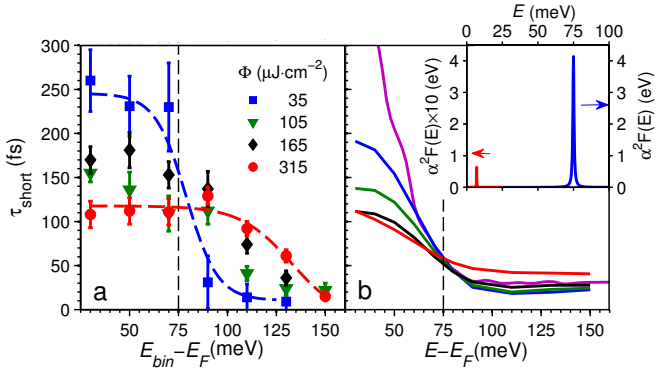

FIG. 4. (color online). a) Experimental $\tau_{\rm short}(E_{\rm bin})$ for $\Phi = 35$ (blue squares), 105 (green triangles), 165 (black diamonds) and 315 (red circles) μJ·cm^{-2}, respectively. Dotted blue and red lines are guides to the eye for the 35 and 315 μJ·cm^{-2} data, respectively. b) Theoretical $\tau_{\rm short}(E_{\rm bin})$ for field strengths of 0.05 (blue), 0.15 (green), 0.25 (black) and 0.50 (red) and equilibrium $\tau_{\rm QP} = \hbar/2{\rm Im}\Sigma$ (purple). The mode energy at 75 meV is marked by the dashed black lines. Inset) (blue, right axis) Theoretical $\alpha^2F(E)$ with electron-boson coupling constant α and dispersion $F(E)$. (red, left axis) The lifetime dampening mode at 15 meV.

includes a weak mode at low energy to prevent an infinite $\tau_{\rm QP}$ within the boson window. ee and impurity scattering are absent from the present model.

Representative $I_{\rm norm}(E_{\rm bin}, t)$ calculated in the time domain are shown in Fig. 3d-f for field strengths comparable to the experiment. They successfully reproduce the reversal of the fastest $\tau_{\rm short}(E_{\rm bin})$ as a function of fluence for $E_{\rm bin}$ above versus below $+\hbar\Omega$. Lacking a true long-time component, these calculated $I_{\rm norm}(E_{\rm bin}, t)$ are fit by single exponentials to produce theoretical $\tau_{\rm short}(E_{\rm bin})$ for several fluences, Fig. 4b. The theoretical $\tau_{\rm short}(E_{\rm bin})$ exhibit the same step at $E - E_{\rm F} \sim +\hbar\Omega$ as the experimental data in Fig. 4a. The theory semiquantitatively captures the increase in $\tau_{\rm short}(E_{\rm bin})$ for $E_{\rm bin} > +\hbar\Omega$ and decrease in $\tau_{\rm short}(E_{\rm bin})$ for $E_{\rm F} < E_{\rm bin} < +\hbar\Omega$. Even the position of the isosbestic point a bit above $+\hbar\Omega$ generated by the increasing pump fluence is captured by the model despite the absence of fluence dependence in the model for the bosonic mode itself. It's remarkable that once the time constant due to boson emission is isolated from other sources of relaxation, its predicted low-fluence-limit equivalence to the relevant term in the equilibrium imaginary part of the self energy ${\rm Im}\Sigma(E)$ naturally emerges [23]. This reflects quantitative agreement between measured and calculated $I_{\rm norm}(E_{\rm bin}, t)$ within the boson window, Fig. 3.

As in the case of the kink's ever more pronounced weakening with increasing pump fluence, the phenomenological model shows how a large redistribution of carrier population acts on the ability of a bosonic mode to assert its presence. By introducing more holes with increasing pump fluence at $-\hbar\Omega < E < E_{\rm F}$ for excited carriers to decay into, carriers at $E_{\rm F} < E < +\hbar\Omega$ relax faster. At the same time, as more empty states are filled for $E_{\rm F} < E < +\hbar\Omega$ by the pump, the ability of carriers excited to $E > +\hbar\Omega$ to decay by emission of a boson of energy $\hbar\Omega$ decreases, leading to an increase in relaxation times [17]. The overall effect is to smooth out the step in population relaxation times at $E - E_{\rm F} \sim +\hbar\Omega$ with increasing fluence.

The vital observation emanating from this comparison of theory and experiment is that a unique timescale for the interaction of excited carriers with a single bosonic mode in Bi2212 is unambiguously separable from the remainder of contributing quasiparticle decay mechanisms above T_c. The coincidence of discontinuous nonequilibrium effects at $\pm\hbar\Omega$ above T_c[15] with the energy scale of the kink at $-\hbar\Omega$ below T_c[5] suggests this mode is present and at least partially coupled to at temperatures much higher than is observed using static ARPES. It's been argued the simultaneous disappearance of the kink's sharpness and emergence of Marginal Fermi Liquid scaling for the self energy when $T > T_c$ evidences coupling of nodal excitations to a spectrum of spin fluctuations[3]. This is opposed to the largely "conventional" appearance of the nodal kink below T_c suggesting an origin in electron-boson coupling. However the binary terms of this debate are perhaps too narrow; whatever the fate of spin fluctuations below T_c, trARPES reveals the bosonic mode $\sim$ 70 meV is itself omnipresent. Taking both points at face value, a plausible explanation for the sum of data is therefore that nodal electrons in Bi2212 couple to both a single pronounced bosonic mode of $\hbar\Omega \sim 70$ meV and a broader spectrum of electronic excitations or other modes, the former much more strongly below T_c, the latter more dominant above[24]. The importance of the kink to the wider high T_c problem might then be seen differently. Understanding why going through T_c has such a profound effect upon which type of nodal coupling is favored may reveal as much or more about the origin of high T_c superconductivity than resolving the couplings themselves.

This work was supported in part by National Science Foundation Grant No. PHYS-1066293 and the hospitality of the Aspen Center for Physics. A.F.K. was supported by the Laboratory Directed Research and Development Program of Lawrence Berkeley National Laboratory under U.S. Department of Energy Contract No. DE-AC02-05CH11231. J.K.F. was supported by the Department of Energy, Office of Basic Energy Sciences, Division of Materials Sciences and Engineering (DMSE) under Contract No. DE-FG02-08ER46542, and by the McDevitt bequest at Georgetown. Computational resources were provided by the National Energy Research Scientific Computing Center supported by the Department of Energy, Office of Science, under Contract No. DE-AC02-05CH11231. Work at Brookhaven National Laboratory was supported by the Center for Emergent Superconductivity, an Energy Frontier Research Center, headquartered at Brookhaven National Laboratory and funded by the U.S. Department of Energy, under Contract No. DE-2009-BNL-PM015. We acknowledge further funding from the Deutsche Forschungsgemeinschaft through SFB 616 and SPP 1458, from the Mercator Research Center Ruhr through Grant No. PR-2011-0003, and from the European Union within the

seventh Framework Program under Grant No. 280555 (GO FAST). We would also like to acknowledge enlightening conversations with Dr. Nick Riviera.

* Direct correspondence to:jrameau@bnl.gov

[1] T. Valla, A. V. Fedorov, P. D. Johnson, B. O. Wells, S. L. Hulbert, Q. Li, G. D. Gu, and N. Koshizuka, Science **285**, 2110 (1999).
[2] A. Lanzara *et al.*, Nature **412**, 510 (2001).
[3] P. D. Johnson *et al.*, Phys. Rev. Lett. **87**, 177007 (2001).
[4] N. C. Plumb *et al.*, New Journal of Physics **15**, 113004 (2013).
[5] J. He *et al.*, Phys. Rev. Lett. **111**, 107005 (2013).
[6] W. Zhang *et al.*, Phys. Rev. Lett. **100**, 107002 (2008).
[7] J. D. Rameau, H.-B. Yang, G. D. Gu, and P. D. Johnson, Phys. Rev. B **80**, 184513 (2009).
[8] T. Valla, T. E. Kidd, W.-G. Yin, G. D. Gu, P. D. Johnson, Z.-H. Pan, and A. V. Fedorov, Phys. Rev. Lett. **98**, 167003 (2007).
[9] A. D. Gromko, A. V. Fedorov, Y.-D. Chuang, J. D. Koralek, Y. Aiura, Y. Yamaguchi, K. Oka, Y. Ando, and D. S. Dessau, Phys. Rev. B **68**, 174520 (2003).
[10] P. W. Anderson, Science **316**, 1705 (2007).
[11] T. P. Devereaux, T. Cuk, Z.-X. Shen, and N. Nagaosa, Phys. Rev. Lett. **93**, 117004 (2004).
[12] P. Dai, H. A. Mook, S. M. Hayden, G. Aeppli, T. G. Perring, R. D. Hunt, and F. Doğan, Science **284**, 1344 (1999).
[13] W. S. Lee *et al.*, Phys. Rev. B **77**, 140504 (2008).
[14] K. Byczuk, M. Kollar, K. Held, Y.-F. Yang, I. A. Nekrasov, T. Pruschke, and D. Vollhardt, Nature Physics **3**, 168 (2007).
[15] J. D. Rameau *et al.*, Phys. Rev. B **89**, 115115 (2014).
[16] W. Zhang *et al.*, Nature Communications **5**, 4959 (2014).
[17] A. F. Kemper, M. A. Sentef, B. Moritz, J. K. Freericks, and T. P. Devereaux, Phys. Rev. B **90**, 075126 (2014).
[18] L. Perfetti, P. A. Loukakos, M. Lisowski, U. Bovensiepen, H. Eisaki, and M. Wolf, Phys. Rev. Lett. **99**, 197001 (2007).
[19] P. S. Kirchman, L. Rettig, D. Nandi, U. Lipowski, M. Wolf, and U. Bovensiepen, Appl. Phys. A **91**, 211 (2008).
[20] M. Eschrig and M. R. Norman, Phys. Rev. Lett. **85**, 3261 (2000).
[21] T. Valla, A. V. Fedorov, P. D. Johnson, and S. L. Hulbert, Phys. Rev. Lett. **83**, 2085 (1999).
[22] N. W. Ashcroft and N. D. Mermin, *Solid State Physics* (Thomson Learning Inc., 1976).
[23] M. Sentef, A. F. Kemper, B. Moritz, J. K. Freericks, Z.-X. Shen, and T. P. Devereaux, Phys. Rev. X **3**, 041033 (2013).
[24] M. R. Norman and A. V. Chubukov, Phys. Rev. B **73**, 140501 (2006).